NANO LETTERS
Cite This: Nano Lett. 2020, 20, 636−643
Letter
pubs.acs.org/NanoLett

Dynamical Control over Terahertz Electromagnetic Interference Shielding with 2D $Ti_3C_2T_y$ MXene by Ultrafast Optical Pulses

Guangjiang Li,[†,#] Naaman Amer,[‡,#] Hassan A. Hafez,[§] Shuohan Huang,[∥] Dmitry Turchinovich,[§] Vadym N. Mochalin,[*,∥,⊥] Frank A. Hegmann,[‡] and Lyubov V. Titova[*,†]

[†]Department of Physics, Worcester Polytechnic Institute, Worcester, Massachusetts 01609, United States
[‡]Department of Physics, University of Alberta, Edmonton, AB T6G 2E1, Canada
[§]Fakultät für Physik, Universität Bielefeld, 33615 Bielefeld, Germany
[∥]Department of Chemistry, Missouri University of Science & Technology, Rolla, Missouri 65409, United States
[⊥]Department of Materials Science & Engineering, Missouri University of Science & Technology, Rolla, Missouri 65409, United States

Supporting Information

ABSTRACT: High electrical conductivity and strong absorption of electromagnetic radiation in the terahertz (THz) frequency range by metallic 2D MXene $Ti_3C_2T_y$ make it a promising material for electromagnetic interference shielding, THz detectors, and transparent conducting electrodes. Here, we demonstrate that ultrafast optical pulses with wavelengths straddling the visible range (400 and 800 nm) induce transient broad-band THz transparency in the MXene that persists for nanoseconds. We demonstrate that optically induced transient THz transparency is independent of temperature from 95 to 290 K. This discovery opens new possibilities for development of switchable electromagnetic interference shielding materials and devices that can be rendered partially transparent on demand for transmitting THz signals, or for designing new THz devices such as sensitive optically gated detectors.

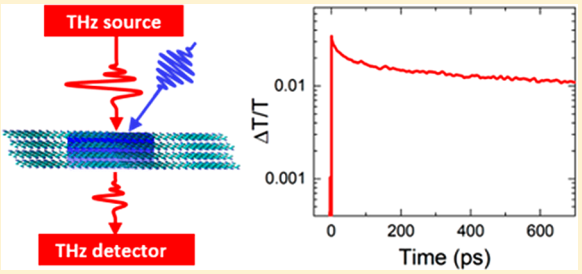

KEYWORDS: *MXene, terahertz spectroscopy, electromagnetic interference shielding, Ti_3C_2, THz, 2D materials*

Two-dimensional (2D) $Ti_3C_2T_y$ is the first discovered member of the MXene family.[1−3] It is synthesized by selective chemical etching of the A element (aluminum) from the hexagonal MAX phase (Ti_3AlC_2).[4] As Al layers are etched away in an aqueous environment, the formed dangling bonds are saturated with O, F, and OH terminations. The resulting nanoflakes (Figure 1a) have a conducting titanium carbide core. Specific terminations, denoted by T_y, and their positions relative to the atoms in Ti_3C_2 sheets influence MXene band structure and electronic properties.[5−10] Since their discovery in 2011, MXenes have shown promise for applications in energy storage, transparent conducting electrodes, photocatalysis, sensors, and saturable absorbers for laser modelocking.[11−19]

Highly conductive and flexible, $Ti_3C_2T_y$ MXene has been recently suggested as a promising material for electromagnetic interference (EMI) shielding in the 8−18 GHz frequency range.[20−24] $Ti_3C_2T_y$ demonstrated EMI shielding efficiency (SE) of >50 dB (dB) for a 2.5-μm film which is superior to graphene, graphite, and copper and aluminum foils.[20,25] The recently reported similarity between the adhesive properties of $Ti_3C_2T_y$ MXene and graphene makes possible layer-by-layer assembly of planar devices combining these two 2D materials for a variety of applications in electronics.[26] An increasing demand for higher bandwidth and rates of data transfer will in the near future shift communications to the higher frequency range, necessitating extending EMI shielding into the newly designated 6G band (up to 3 THz) where international standards for EMI are yet to be formulated.[27−30]

Here, we focus on EMI shielding properties of $Ti_3C_2T_y$ in the THz frequency range. $Ti_3C_2T_y$ has been theoretically predicted[31,32] and experimentally demonstrated to be highly sensitive to the THz radiation.[31,33] We have also reported a surprising effect that photoexcitation with near-infrared (800 nm) pulses suppresses conductivity in the MXene for hundreds of picoseconds.[33] That discovery led us to the idea of using optical pulses to control the extent of EMI shielding by $Ti_3C_2T_y$ MXene. As reported below, the highly conductive $Ti_3C_2T_y$ has EMI shielding efficiency in the THz range as high as ~2.5 dB for the sample as thin as only 25 nm, corresponding to a specific shielding efficiency per unit thickness of ca. 4×10^5 dB cm^2 g^{-1}. Stemming from a combination of absorption and reflection losses, including multiple internal reflections between the individual highly conductive $Ti_3C_2T_y$ nanosheets within a film, EMI SE is expected to scale with the film

Received: October 24, 2019
Revised: December 10, 2019
Published: December 11, 2019

DOI: 10.1021/acs.nanolett.9b04404
Nano Lett. 2020, 20, 636−643

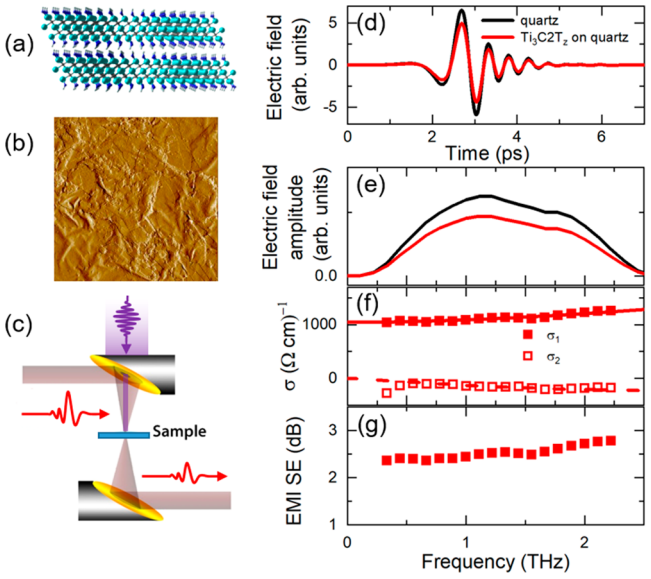

Figure 1. (a) Schematic representation of a $Ti_3C_2T_y$ film: five atomic layer thick Ti_3C_2 cores of individual flakes are terminated by − OH (shown), −F, or =O groups. (b) 2 μm by 2 μm AFM micrograph of a 25 nm thick $Ti_3C_2T_y$ film. (c) THz spectroscopy experiment. (d) THz probe pulse transmitted through a quartz substrate and through the substrate with a $Ti_3C_2T_y$ film. (e) Corresponding THz electric field amplitude, (f) complex THz conductivity (solid symbols represent real and open symbols−imaginary conductivity components; lines show a global fit of both components to the Drude-Smith model). (g) EMI SE calculated from data in (e).

thickness and can potentially reach tens of dB for films that are several micrometers thick.[20,34] Furthermore, it can be further enhanced by depositing $Ti_3C_2T_y$ films on nanoslot antenna arrays, resulting in EMI SE of over 20 dB at 1 THz for films with a thickness of only 150 nm.[31] In this report, we show that both 800 nm (1.55 eV) and 400 nm (3.1 eV) optical excitation pulses result in a transient suppression of THz absorption that lasts over nanoseconds. This possibility of dynamically opening a few nanoseconds wide transmission window in otherwise THz opaque material is of great interest for applications such as tunable EMI shielding, where on-demand transparency for transmitting signals may be desirable. We discuss possible mechanisms behind this phenomenon and anticipate that this work will not only inspire practical applications of metallic MXenes in THz devices but also provide critical experimental inputs to developing a comprehensive theoretical description of the electronic and optical properties of MXenes, as well as impetus for further understanding of the contribution of the surface terminations to these properties.

EXPERIMENTAL METHODS

Fabrication of $Ti_3C_2T_y$ Film. $Ti_3C_2T_y$ was synthesized by selective etching of aluminum atomic layers in Ti_3AlC_2 MAX phase by the MILD etching method as described previously.[11,20,35] MXene thin film on quartz was fabricated from a concentrated $Ti_3C_2T_y$ colloidal solution via the interfacial film deposition method.[13] About 100 μL of $Ti_3C_2T_y$ colloidal solution were mixed in 50 mL of DI water together with 5 mL of toluene added dropwise over 5−10 min of stirring. The dispersion was then poured directly into a beaker filled with 400 mL of DI water, and a piece of quartz substrate, hydrophilized using Piranha solution (3 mL of 30% H_2O_2 + 9 mL of 98% H_2SO_4), was placed at the bottom. After ∼15 min, MXene film self-assembled between water and toluene. Quartz substrate was slowly lifted from the solution through the interface, forming a 25 ± 5 nm-thick film, as determined by profilometry (Figure S1). A representative atomic force microscopy (AFM) image of the film (Figure 1b) shows that the film is continuous and consists of overlapping nanoflakes of sub μm lateral dimensions. The AFM image was acquired using Park NX20 AFM operated in tapping mode. Optical transmission of the film varies between 60% and 70% in the 400−900 nm range, suggesting a significant absorption despite the small thickness (Figure S2).

THz Spectroscopy. We investigated properties of the $Ti_3C_2T_y$ film using THz spectroscopy in the transmission configuration, as illustrated in Figure 1c.[36−38] THz probe pulses were generated by optical rectification of 100 fs, 800 nm pulses in 1 mm thick [110] ZnTe crystal and focused to an ∼1.5 mm diameter spot on the sample with an off-axis parabolic mirror. Transmitted THz pulses were coherently detected using free-space electrooptic sampling in a second 1 mm thick [110] ZnTe crystal. To examine the effect of photoexcitation on THz conductivity, we have carried out optical pump−THz probe measurements, in which the sample was excited by 100 fs, 800 or 400 nm pulses at normal incidence via a hole in the parabolic mirror, as shown in Figure 1c.[38−42]

X-ray Photoelectron Spectroscopy. X-ray photoelectron spectroscopy (XPS) measurements of $Ti_3C_2T_y$ MXene were performed using a KRATOS AXIS 165 X-ray photoelectron spectrometer with a monochromatic Al X-ray source. XPS investigation was performed to characterize the surface chemistry of the prepared $Ti_3C_2T_y$ MXene.

RESULTS AND DISCUSSION

The ∼25 nm-thick $Ti_3C_2T_y$ film significantly attenuates broadband, picoseconds long THz pulses (Figure 1). From the THz amplitude attenuation (Figure 1e), we calculate the absorption coefficient of the film to be $\sim 2.2 \times 10^5$ cm^{-1} in the THz range (Figure S3). By comparing the amplitude and the phase of the THz pulses transmitted through the substrate alone and the sample on a substrate in the frequency domain, we calculate the complex THz conductivity ($\tilde{\sigma}(\omega)$) of the film using the relation $\frac{\tilde{E}_{sample}(\omega)}{\tilde{E}_{substrate}(\omega)} = \frac{n+1}{n+1+Z_0\tilde{\sigma}(\omega)}$, where Z_0 = 377 Ω is the impedance of the free space and n is the refractive index of the quartz substrate in the THz range.[38] The complex conductivity spectrum is shown in Figure 1f, and the corresponding complex permittivity is given in Figure S4. As reported earlier,[33] the real conductivity in $Ti_3C_2T_y$ films is suppressed at low frequencies by the interflake barriers and can be described by a Drude−Smith model, a modification of the free carrier Drude conductivity that accounts for localization of the mobile carriers on the length scales commensurate with their mean free path.[36,41,43−50] The Drude−Smith complex frequency-resolved conductivity is given as $\tilde{\sigma}(\omega) = \frac{\sigma_0}{1-i\omega\tau_{DS}}\left(1+\frac{c}{1-i\omega\tau_{DS}}\right)$ where $\sigma_0 = \frac{Ne^2\tau_{DS}}{m^*}$ is the Drude weight, τ_{DS} is a carrier scattering time, N is the charge carrier density, and m^* is the carrier effective mass. The phenomenological c parameter, which can vary in the $-1 \le c \le 0$ range, represents the impact of barriers such as nanoflake edges and defects on long-range carrier transport. When c = 0, carriers follow the classical Drude model of free electron gas

DOI: 10.1021/acs.nanolett.9b04404
Nano Lett. 2020, 20, 636−643

conduction, and when $c = -1$, they are fully localized over the short distances, resulting in complete suppression of conductivity at $\omega = 0$. Compared to the film used in our previous work,[33] the $Ti_3C_2T_y$ film studied here is continuous, consisting of larger overlapping flakes, which is reflected in a much less negative c-parameter (−0.68 vs −0.97) and an ∼4 times larger DC conductivity $\sigma_{DC} \approx 1250\ (\Omega\ cm)^{-1}$. Using a zone-center electron effective mass of $0.2845m_e$,[51] we find that the intrinsic carrier density is large, $\sim 2 \times 10^{21}\ cm^{-3}$, in agreement with the value determined from electrical measurements on $Ti_3C_2T_y$ films.[52] From the scattering time (19 ± 1 fs), we calculate the intrinsic carrier mobility, or mobility of carriers over the mesoscopic length scales within individual flakes, to be $\mu_{intrinsic} = \frac{e\tau_{DS}}{m^*} \approx 110\ cm^2/(V\ s)$. We find that high free carrier density and conductivity result in the high EMI shielding efficiency (SE), defined as $-20\log\left(\frac{E_{sample}}{E_{substrate}}\right)$, as shown in Figure 1g. It should be noted that EM shielding by thin conductive films occurs due to a combination of reflection and absorption losses experienced by the EM radiation, and the reported total EMI SE contains both contributions. At ∼2.5 dB for a 25 nm film, it is comparable to the SE reported for carbon nanotube films and composites, multilayer graphene, and to the high THz EMI SE that has been reported recently for metallic MXenes.[31,53,54] The relatively low density of $Ti_3C_2T_y$ (ca. 2.39 g cm^{-3})[20] makes it particularly attractive for EMI SE applications, as high SE can be achieved without adding much extra weight to devices that are being shielded. A figure of merit used to evaluate the suitability of the material for applications where weight is relevant (such as aerospace applications) is specific SE (SSE) per unit thickness, defined as SE divided by density and thickness. We find that SSE/thickness for $Ti_3C_2T_y$ in the THz range is very high at $\sim 4 \times 10^5$ dB $cm^2\ g^{-1}$ (Figure S3). Although not many reports exist on EMI SE characteristics of materials in the THz range, making comparison to accepted standard THz EMI shielding materials impossible, this number is 1−2 orders of magnitude higher than that for metals (Al, Cu) in the GHz range.[20]

Having established that the 25 nm thick $Ti_3C_2T_y$ has excellent THz shielding properties, we now turn to the main subject of this report, which is manipulation of EMI SE in the THz range by optical excitation. We find that both 800 and 400 nm light pulses *enhance transmission* of the THz pulses. The overall dynamics of this phenomenon are represented by the relative change in transmission of the THz probe pulse peak (Figure 2). As shown in Figure 3, the frequency-resolved transient change in EMI SE at different times after excitation with 800 nm pulse in reveals that EMI SE is suppressed over the entire bandwidth of the THz probe (0.25−2.25 THz), with the magnitude of the effect exhibiting a slow monotonous increase with frequency. This EMI SE suppression is a direct result of the photoinduced transient decrease in the real conductivity component σ_1 over the entire experimental frequency range (Figure S5), as the power absorption of electromagnetic radiation is directly proportional to the real part of the conductivity in the corresponding frequency range.[55]

We now turn to the dynamics of the observed suppression of conductivity and EMI SE as represented by the transient increase in the THz probe pulse transmission (Figure 2). Following a fast rise immediately after the optical excitation at $t = 0$, photoinduced THz transparency decays over the next

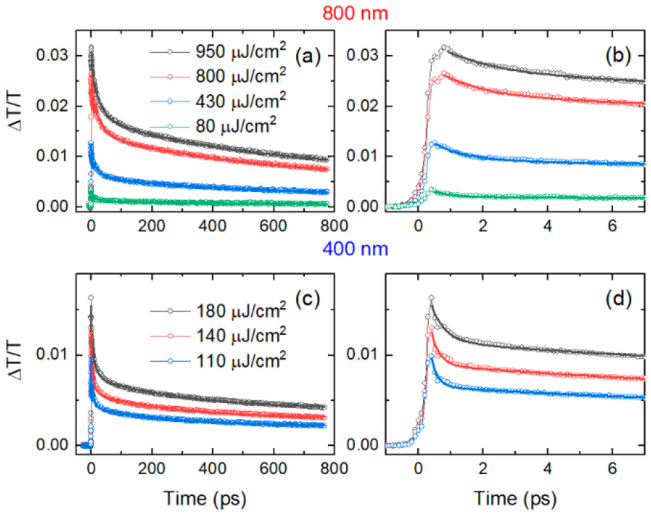

Figure 2. (a) Photoinduced change in the THz peak transmission as a function of time after photoexcitation with 800 nm (a, b) and 400 nm (c, d) pulses with excitation fluence values given in the legends. Panels (b) and (d) show expanded views of the initial decay profiles in (a) and (c). Thick solid lines are fits of the experimental data to the multiexponential decays.

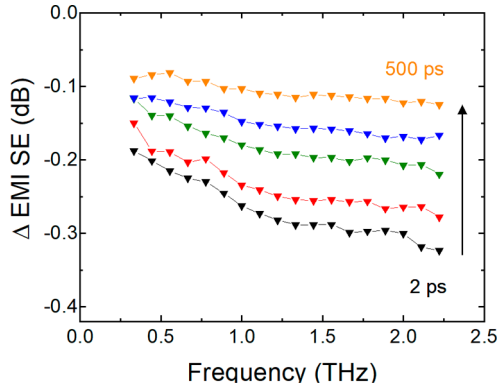

Figure 3. Photoinduced change in EMI SE at different times following excitation with 800 nm, 950 $\mu J/cm^2$ pulse.

hundreds of picoseconds, and the decay dynamics differ for 800 and 400 nm excitation. For the purpose of drawing comparisons between the effects of the two excitation wavelengths, we fit the experimental data in Figure 2 to a multiexponential decay function. We find that including three decaying terms and a constant adequately captures the dynamics of the transient change in transmission within the experimental time window. Thus, the solid lines in Figure 2 are fits of the experimental data using the function $\frac{\Delta T(t)}{T} = A_0 + A_1\exp\left(-\frac{t}{t_1}\right) + A_2\exp\left(-\frac{t}{t_2}\right) + A_3\exp\left(-\frac{t}{t_3}\right)$, where t_1, t_2, and t_3 are decay times, A_1, A_2, and A_3 are the corresponding amplitudes, and A_0 is the amplitude of transient component or components with long, >1 ns decay times that cannot be accurately determined from our data. A summary of the fitting results for both 800 and 400 nm excitation is presented in Figure 4 and Figure S6. The following observations can be made:

For both 800 and 400 nm pump excitations, the peak of transmission enhancement is linearly dependent on the excitation fluence in the fluence range studied here. On this conjuncture it is worth comparing the magnitude of the

DOI: 10.1021/acs.nanolett.9b04404
Nano Lett. 2020, 20, 636−643

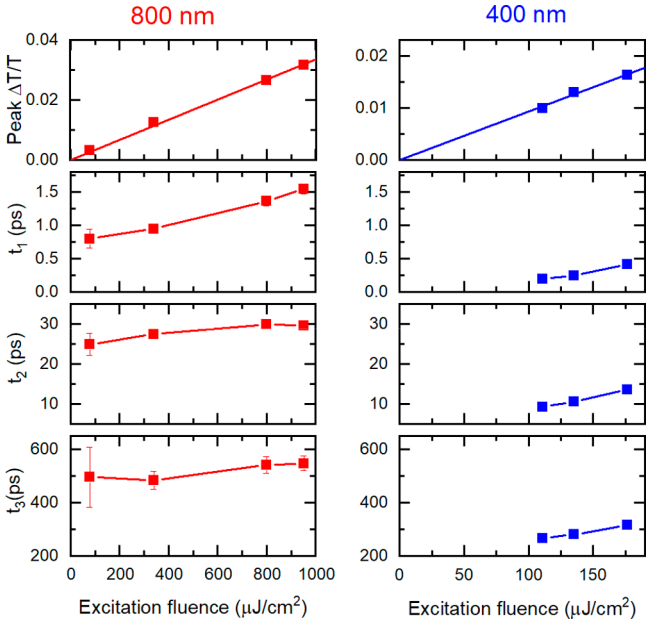

Figure 4. Fitting parameters resulting from fitting transient photoinduced THz probe peak transmission enhancement to a three exponential decay function: peak and decay times for 800 nm excitation (left, red symbols) and 400 nm excitation (right, blue symbols).

transient THz transparency observed here to that observed in the earlier work where a slightly thinner (~16 nm), less continuous film with nearly four times lower DC conductivity was used.[33] We find that, for similar excitation fluence with a 800 nm optical pump, the peak of $\Delta T/T$ is nearly twice as large in the present study, suggesting that the magnitude of transient conductivity suppression is a function of not only MXene film thickness but also film conductivity.

By examining the excitation fluence dependence of the transient THz transparency dynamics, we find that the three decay times, t_1, t_2, and t_3, become longer with increasing excitation fluence. The three measured decay times are shorter for 400 nm excitation compared to 800 nm. The relative contribution of the fastest decay to the relaxation of the photoinduced conductivity suppression, 0.6−1.6 ps for 800 nm excitation and 0.2−0.4 ps for 400 nm, decreases with increasing fluence (Figure S6). If this fast decay is associated with relaxation of certain photoexcited states, which are yet to be identified, this observation would suggest that the density of those states is limited. This effect is more pronounced for 400 nm excitation.

To understand the mechanism responsible for this long-lived suppression of conductivity in a thin metallic MXene film that results in the observed enhancement of THz transmission, we turn to reports on other metallic systems that exhibit similar phenomena.

The response of metals to an ultrafast optical excitation is vastly different from that of semiconductors. In semiconductors, the dominant effect of photoexcitation is an increase in carrier density and, consequently, positive photoconductivity. At a high photoexcited carrier density, an increase in conductivity in semiconductors due to injection of carriers is tempered by the reduction of mobility due to enhanced carrier−carrier scattering.[56] Transient conductivity changes in metals result from a combined effect of intraband and interband transitions, with interband excitations playing a dominant role for photon energy above the interband transition threshold.[57−59] However, the interband excitation of a metal often does not lead to a significant change in the free carrier density. In this case, the sign of the photoinduced conductivity change is typically negative, as it is dominated by a reduction of carrier mobility in response to the increase in carrier and lattice temperature.[48,60] Ultrafast optical excitation generates a highly nonequilibrium population of electrons which rapidly (over subpicosecond time scales) equilibrate by electron−electron scattering and form a Fermi distribution with a collective hot electron temperature T_e that can reach thousands of Kelvin above the lattice temperature.[57,58,61] Over the next ~1−10 ps time period, hot carrier bath cools and equilibrates with the lattice by carrier-phonon scattering. At this point, an increased lattice temperature is responsible for the reduction in the electrical conductivity. The final stage of the recovery after ultrafast optical excitation is significantly slower (time scale ≈ hundreds of picoseconds),[57,58] as it is driven by the lattice temperature gradients that form in the sample and is limited by the phonon diffusion. If the film thickness is on the order of the optical penetration depth and/or hot carrier diffusion length, then the final relaxation is limited by the thermal boundary resistance between the film and the substrate that supports it. Among 2D materials, reduction of conductivity after interband excitation with ultrashort optical pulses has been observed in highly doped or gated graphene and explained by redistribution of energy from photoexcited electron−hole pairs to initially unexcited free electrons, resulting in their heating via either the direct conversion of excess energy into electronic heat or its dissipation into optical phonons.[62−64] The resulting reduction in conductivity recovers in ~2 ps, several orders of magnitude faster than the recovery time we observe in $Ti_3C_2T_y$ film.

For the ~25 nm thick MXene film composed of metallic $Ti_3C_2T_y$ nanoflakes, the transient conductivity suppression with excitation energies of 1.55 eV (800 nm) and 3.1 eV (400 nm) results in both intra- and interband carrier excitations that contribute to hot carrier generation by promoting carriers from the Fermi energy E_F into higher energy states (former) or by generating new electron−hole pairs (latter). Carrier−carrier scattering then establishes a hot carrier distribution with carrier temperature T_C that is higher than the lattice temperature T_L, followed by a rapid (approximately picoseconds) equilibration of carrier and lattice temperature via the carrier-phonon scattering. The typical time scales for these processes are commensurate with the observed fast relaxation process t_1, suggesting that the initial fast recovery of conductivity suppression might indeed be due to the combined effect of these processes, i.e., carrier−carrier and carrier−lattice thermalization. The difference in t_1 for 400 and 800 nm excitation may then be explained by the dependence of the scattering rates on carrier excess energy, while lower t_1 at increased fluence may result from a more efficient screening of carrier−lattice interactions at higher carrier density.[65]

Ultimately, the end result of carrier−carrier and carrier−lattice equilibration, occurring over the first few picoseconds following ultrafast optical excitation, is an increased lattice temperature. How quickly does the film return to the ambient temperature, and is this laser-induced transient heating responsible for the observed long-lived conductivity suppression in a $Ti_3C_2T_y$ film?

DOI: 10.1021/acs.nanolett.9b04404
Nano Lett. 2020, 20, 636−643

The thermal properties of $Ti_3C_2T_y$ films are still largely unexplored. A specific heat in the range 1.1−1.5 MJ m^{-3} K, depending on termination T_y, has been theoretically calculated for an isolated monolayer.[66] Measurements of thermal conductivity, which determines how quickly the photoexcited area would cool to ambient temperature, vary from 2.84 to 55.8 W m^{-1} K^{-1}.[67,68] Thermal boundary conductance at ambient temperature between a $Ti_3C_2T_y$ film and a substrate, which governs heat flow from the photoexcited film to a substrate, has been recently reported for the $Ti_3C_2T_y$/SiO2/Si interface to vary from 10 to 27 MW m^{-2} K^{-1} depending on the presence of absorbents.[69]

Temperature-dependent measurements of electrical conductivity of $Ti_3C_2T_y$ films have shown that conductivity either remains unchanged when the temperature is varied from 80 K to room temperature or increases by only a few percent with increasing temperature.[3,5,67] The insensitivity of conductivity to the lattice temperature casts doubts over the thermal origin of the observed long-lived conductivity suppression following the photoexcitation.

To shed more light on this, we have carried out THz-TDS and optical (800 nm) pump-THz probe spectroscopy measurements at 95 K. We find that EMI SE at 95 K is the same as at room temperature (Figure 5a), as the real THz

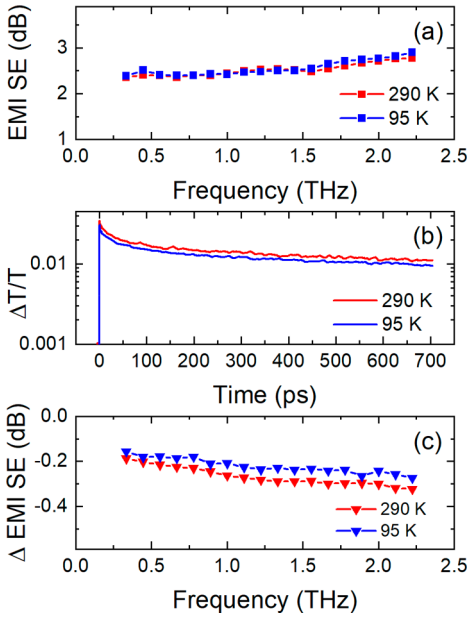

Figure 5. (a) EMI SE at 290 and 95 K. (b) Transient change in transmission of THz probe pulse peak after excitation with 800 nm, 950 $\mu J/cm^2$ pulse at 290 and 95 K. (c) Change in EMI SE 2 ps after photoexcitation at 290 and 95 K with 800 nm, 950 $\mu J/cm^2$ pulse.

conductivity component exhibits no change when the film temperature is reduced from 290 to 95 K (Figure S7). This finding is in agreement with conventional temperature-dependent measurements of $Ti_3C_2T_y$ DC conductivity.[3,5,67] The unexpected finding is that of the insensitivity of the optical excitation-induced reduction in EMI SE and its relaxation dynamics to a temperature change from 290 to 95 K (Figure 5b, 5c and Figure S8). This result effectively rules out the slow cooling of the photoexcited film by transferring heat to the substrate or laterally, to unexcited portions of the film, as a reason for the slow relaxation of the optically induced THz transparency. Parameters such as thermal conductivity and thermal boundary conductance are expected to be temperature dependent, and in fact, the study that found little to no change in the electrical conductivity between 95 and 290 K also found that the thermal conductivity changes by more than a factor of 2.[67] We therefore conclude that, while the lattice temperature must be increased by the photoexcitation, it does not play a major role in conductivity suppression in metallic MXenes, unlike conventional metals, and cannot explain the observed phenomenon of transient conductivity suppression by optical pulses.

Additional experiments as well as theoretical investigations of the ultrafast photoexcitations in metallic MXenes are necessary to uncover the mechanisms reponsible for this remarkably long-lived conductivity suppression and reduction of EMI SE. With future studies in mind, we put forth the following hypothesis: the complete picture of the photo-induced effects in MXenes must necessarily consider the role played by the terminations, T_y (F, OH, O, and their combinations). Multiple theoretical studies showed that MXene surface chemistry plays an important role in transport properties.[5−8,70,71] Specifically, fluorine enhances conductivity compared to the bare Ti_3C_2 by introducing additional extended electronic states outside titanium carbide cores, while the termination of the surface by oxygen introduces localized states near the oxygen and carbon atoms and reduces overall conductivity.[6−8] Moreover, since MXenes are reactive toward water, their surface chemistry and composition may change over time.[72] DFT calculations have also shown that optical absorption in the 1.0−4.5 eV range is significantly lower in F and OH terminated Ti_3C_2 compared to the bare and O-terminated one.[9] Typically, $Ti_3C_2T_y$ features a combination of all of these terminations. It is then possible that optical excitation with 1.55 eV (800 nm) or 3.1 eV (400 nm) photons excites some of the localized states associated with specific surface terminating groups. The resulting localized charges on the nanoflake surface change the electrostatic potential profile within the conductive cores, which has been theoretically predicted to impact transport properties.[6] The origin of the long-lived conductivity suppression may be the relaxation of those localized surface excitations occurring over hundreds of picosecond or longer. Differences in optical absorption at 400 and 800 nm for different surface-related localized states may then explain the variation in relaxation dynamics of conductivity suppression for these two excitation wavelengths, while the slowing of the relaxation at higher excitation fluence may turn out to result from saturation of the intermediate states that take part in relaxation. In our $Ti_3C_2T_y$, a mix of −OH, −O−, and −F terminations is present, as evident from XPS studies (Supplementary Figure S8 and Table S1). While MXene films with homogeneous terminations are yet to be demonstrated, several approaches to tailoring the nature of terminations by treating as-synthesized MXenes with bases such as NaOH or LiOH to replace −F terminations with −OH or with acids such as HCl to attach trace −Cl are now being developed.[73,74] Thus, the future experimental studies with $Ti_3C_2T_y$ films with specific, well-defined surface terminations, as well as more detailed theoretical investigations of their optical and transport properties, will resolve the unanswered questions about the role of terminations in optically induced enhanced THz transmission.

In conclusion, we find that flexible and solution-processable thin $Ti_3C_2T_y$ films have high THz conductivity and exhibit

DOI: 10.1021/acs.nanolett.9b04404
Nano Lett. 2020, 20, 636−643

highly efficient EMI shielding properties in the THz range. Their shielding efficiency can be reduced on demand for nanoseconds-long time periods by ultrashort optical pulses, a functionality that is independent of temperature from at least 95 K to the room temperature. These unique properties make $Ti_3C_2T_y$ Mxene promising for THz EMI shielding where dynamical control over the SE is needed, such as when it is desirable to open on-demand THz communication channels. A transient increase in THz transmission by a few percent may be sufficient for short-range point-to-point communications that are now envisioned for THz communications.[75] Another area where applications are possible is in THz devices. For example, on demand optically gated THz transparency may be required for sensitive THz detectors. The flexibility of $Ti_3C_2T_y$ and other MXenes and their compatibility with a variety of substrates further add to the attractiveness of this emergent class of 2D materials for applications in THz technology and EMI shielding applications.

■ ASSOCIATED CONTENT

Supporting Information

The Supporting Information is available free of charge at https://pubs.acs.org/doi/10.1021/acs.nanolett.9b04404.

Film thickness and UV−vis transmittance measurements, calculated THz absorbance and the corresponding specific EMI SE per unit thickness, complex permittivity of the MXene film at room temperature, photoinduced change in complex conductivity as a function of time after photoexcitation, fitting parameters resulting from fitting transient THz transmission enhancement to a multiexponential decay, complex THz conductivity of the MXene film at room temperature and at 95 K, photoinduced changes in complex conductivity and EMI SE at 95 K, and a summary of XPS investigation (PDF)

■ AUTHOR INFORMATION

Corresponding Authors

*mochalinv@mst.edu.

*ltitova@wpi.edu.

ORCID

Vadym N. Mochalin: 0000-0001-7403-1043

Lyubov V. Titova: 0000-0002-2146-9102

Author Contributions

#G.L. and N.A. contributed equally.

Notes

The authors declare no competing financial interest.

■ ACKNOWLEDGMENTS

G.L. thanks Worcester Polytechnic Institute PhD Global Research Experience award. We thank Helma Burg for help with profilometer measurements and Uwe Rietzler for help with AFM measurements. D.T. acknowledges the project "Nonequilibrium dynamics in solids probed by terahertz fields" funded by the Deutsche Forschungsgemeinschaft (DFG, German Research Foundation) − Projektnummer 278162697 − SFB 1242. N.A. and F.A.H. acknowledge support from NSERC, CFI, and the Alberta Innovates Strategic Chairs Program, and technical support from B. Shi. This material is based upon work supported by the National Science Foundation under Grant No. 1930881 CMMI.

■ REFERENCES

(1) Naguib, M.; Mashtalir, O.; Carle, J.; Presser, V.; Lu, J.; Hultman, L.; Gogotsi, Y.; Barsoum, M. W. Two-Dimensional Transition Metal Carbides. *ACS Nano* **2012**, *6* (2), 1322−1331.

(2) Ghidiu, M.; Lukatskaya, M. R.; Zhao, M.-Q.; Gogotsi, Y.; Barsoum, M. W. Conductive two-dimensional titanium carbide 'clay' with high volumetric capacitance. *Nature* **2014**, *516*, 78.

(3) Halim, J.; Lukatskaya, M. R.; Cook, K. M.; Lu, J.; Smith, C. R.; Näslund, L.-Å.; May, S. J.; Hultman, L.; Gogotsi, Y.; Eklund, P.; Barsoum, M. W. Transparent Conductive Two-Dimensional Titanium Carbide Epitaxial Thin Films. *Chem. Mater.* **2014**, *26* (7), 2374−2381.

(4) Naguib, M.; Mochalin, V. N.; Barsoum, M. W.; Gogotsi, Y. 25th Anniversary Article: MXenes: A New Family of Two-Dimensional Materials. *Adv. Mater.* **2014**, *26* (7), 992−1005.

(5) Hart, J. L.; Hantanasirisakul, K.; Lang, A. C.; Anasori, B.; Pinto, D.; Pivak, Y.; van Omme, J. T.; May, S. J.; Gogotsi, Y.; Taheri, M. L. Control of MXenes' electronic properties through termination and intercalation. *Nat. Commun.* **2019**, *10* (1), 522.

(6) Berdiyorov, G. R. Effect of surface functionalization on the electronic transport properties of Ti3C2MXene. *EPL (Europhysics Letters)* **2015**, *111* (6), 67002.

(7) Schultz, T.; Frey, N. C.; Hantanasirisakul, K.; Park, S.; May, S. J.; Shenoy, V. B.; Gogotsi, Y.; Koch, N. Surface Termination Dependent Work Function and Electronic Properties of Ti3C2Tx MXene. *Chem. Mater.* **2019**, *31*, 6590.

(8) Khazaei, M.; Ranjbar, A.; Arai, M.; Sasaki, T.; Yunoki, S. Electronic properties and applications of MXenes: a theoretical review. *J. Mater. Chem. C* **2017**, *5* (10), 2488−2503.

(9) Bai, Y.; Zhou, K.; Srikanth, N.; Pang, J. H. L.; He, X.; Wang, R. Dependence of elastic and optical properties on surface terminated groups in two-dimensional MXene monolayers: a first-principles study. *RSC Adv.* **2016**, *6* (42), 35731−35739.

(10) Xie, Y.; Naguib, M.; Mochalin, V. N.; Barsoum, M. W.; Gogotsi, Y.; Yu, X.; Nam, K.-W.; Yang, X.-Q.; Kolesnikov, A. I.; Kent, P. R. C. Role of Surface Structure on Li-Ion Energy Storage Capacity of Two-Dimensional Transition-Metal Carbides. *J. Am. Chem. Soc.* **2014**, *136* (17), 6385−6394.

(11) Anasori, B.; Lukatskaya, M. R.; Gogotsi, Y. 2D metal carbides and nitrides (MXenes) for energy storage. *Nature Reviews Materials* **2017**, *2*, 16098. https://www.nature.com/articles/natrevmats201698#supplementary-information

(12) Chaudhari, N. K.; Jin, H.; Kim, B.; Baek, D. S.; Joo, S. H.; Lee, K. MXene: an emerging two-dimensional material for future energy conversion and storage applications. *J. Mater. Chem. A* **2017**, *5* (47), 24564−24579.

(13) Dong, Y.; Chertopalov, S.; Maleski, K.; Anasori, B.; Hu, L.; Bhattacharya, S.; Rao, A. M.; Gogotsi, Y.; Mochalin, V. N.; Podila, R. Saturable Absorption in 2D Ti_3C_2 MXene Thin Films for Passive Photonic Diodes. *Adv. Mater.* **2018**, *30* (10), 1705714.

(14) Guo, Z. L.; Zhou, J.; Zhu, L. G.; Sun, Z. M. MXene: a promising photocatalyst for water splitting. *J. Mater. Chem. A* **2016**, *4* (29), 11446−11452.

(15) Jhon, Y. I.; Koo, J.; Anasori, B.; Seo, M.; Lee, J. H.; Gogotsi, Y.; Jhon, Y. M. Metallic MXene Saturable Absorber for Femtosecond Mode-Locked Lasers. *Adv. Mater.* **2017**, *29* (40), 1702496.

(16) Lee, E.; Mohammadi, A. V.; Prorok, B. C.; Yoon, Y. S.; Beidaghi, M.; Kim, D. J. Room Temperature Gas Sensing of Two-Dimensional Titanium Carbide (MXene). *ACS Appl. Mater. Interfaces* **2017**, *9* (42), 37184−37190.

(17) Wang, C.; Peng, Q. Q.; Fan, X. W.; Liang, W. Y.; Zhang, F.; Liu, J.; Zhang, H. MXene Ti3C2Tx saturable absorber for pulsed laser at 1.3 mu M. *Chin. Phys. B* **2018**, *27* (9), 094214.

(18) Zhang, C.; Anasori, B.; Seral-Ascaso, A.; Park, S. H.; McEvoy, N.; Shmeliov, A.; Duesberg, G. S.; Coleman, J. N.; Gogotsi, Y.; Nicolosi, V. Transparent, Flexible, and Conductive 2D Titanium Carbide (MXene) Films with High Volumetric Capacitance. *Adv. Mater.* **2017**, *29* (36), 1702678.

DOI: 10.1021/acs.nanolett.9b04404
Nano Lett. 2020, 20, 636−643

(19) Chertopalov, S.; Mochalin, V. N. Environment-Sensitive Photoresponse of Spontaneously Partially Oxidized Ti3C2MXene Thin Films. *ACS Nano* **2018**, *12* (6), 6109−6116.
(20) Shahzad, F.; Alhabeb, M.; Hatter, C. B.; Anasori, B.; Man Hong, S.; Koo, C. M.; Gogotsi, Y. Electromagnetic interference shielding with 2D transition metal carbides (MXenes). *Science* **2016**, *353* (6304), 1137−1140.
(21) Hu, S.; Li, S.; Xu, W.; Zhang, J.; Zhou, Y.; Cheng, Z. Rapid preparation, thermal stability and electromagnetic interference shielding properties of two-dimensional Ti3C2MXene. *Ceram. Int.* **2019**, *45* (16), 19902−19909.
(22) Li, X.; Yin, X.; Liang, S.; Li, M.; Cheng, L.; Zhang, L. 2D carbide MXene Ti2CTX as a novel high-performance electromagnetic interference shielding material. *Carbon* **2019**, *146*, 210−217.
(23) He, P.; Wang, X.-X.; Cai, Y.-Z.; Shu, J.-C.; Zhao, Q.-L.; Yuan, J.; Cao, M.-S. Tailoring Ti3C2Tx nanosheets to tune local conductive network as an environmentally friendly material for highly efficient electromagnetic interference shielding. *Nanoscale* **2019**, *11* (13), 6080−6088.
(24) Liu, J.; Liu, Z.; Zhang, H.-B.; Chen, W.; Zhao, Z.; Wang, Q.-W.; Yu, Z.-Z. Ultrastrong and Highly Conductive MXene-Based Films for High-Performance Electromagnetic Interference Shielding. *Advanced Electronic Materials* **2019**, 1901094.
(25) Feng, W.; Luo, H.; Wang, Y.; Zeng, S.; Deng, L.; Zhou, X.; Zhang, H.; Peng, S. Ti3C2MXene: a promising microwave absorbing material. *RSC Adv.* **2018**, *8* (5), 2398−2403.
(26) Li, Y.; Huang, S.; Wei, C.; Wu, C.; Mochalin, V. N. Adhesion of two-dimensional titanium carbides (MXenes) and graphene to silicon. *Nat. Commun.* **2019**, *10* (1), 3014.
(27) Ma, J.; Shrestha, R.; Adelberg, J.; Yeh, C.-Y.; Hossain, Z.; Knightly, E.; Jornet, J. M.; Mittleman, D. M. Security and eavesdropping in terahertz wireless links. *Nature* **2018**, *563* (7729), 89−93.
(28) Kürner, T.; Priebe, S. Towards THz Communications - Status in Research, Standardization and Regulation. *J. Infrared, Millimeter, Terahertz Waves* **2014**, *35* (1), 53−62.
(29) Akyildiz, I. F.; Jornet, J. M.; Han, C. Terahertz band: Next frontier for wireless communications. *Physical Communication* **2014**, *12*, 16−32.
(30) Federici, J.; Moeller, L. Review of terahertz and subterahertz wireless communications. *J. Appl. Phys.* **2010**, *107* (11), 111101.
(31) Choi, G.; Shahzad, F.; Bahk, Y. M.; Jhon, Y. M.; Park, H.; Alhabeb, M.; Anasori, B.; Kim, D. S.; Koo, C. M.; Gogotsi, Y.; Seo, M. Enhanced Terahertz Shielding of MXenes with Nano-Metamaterials. *Adv. Opt. Mater.* **2018**, *6* (5), 1701076.
(32) Jhon, Y. I.; Seo, M.; Jhon, Y. M. First-principles study of a MXene terahertz detector. *Nanoscale* **2018**, *10* (1), 69−75.
(33) Li, G.; Kushnir, K.; Dong, Y.; Chertopalov, S.; Rao, A. M.; Mochalin, V. N.; Podila, R.; Titova, L. V. Equilibrium and non-equilibrium free carrier dynamics in 2D Ti 3 C 2 T x MXenes: THz spectroscopy study. *2D Mater.* **2018**, *5* (3), No. 035043.
(34) Hantanasirisakul, K.; Gogotsi, Y. Electronic and Optical Properties of 2D Transition Metal Carbides and Nitrides (MXenes). *Adv. Mater.* **2018**, *30* (52), 1804779.
(35) Lipatov, A.; Alhabeb, M.; Lukatskaya, M. R.; Boson, A.; Gogotsi, Y.; Sinitskii, A. Effect of Synthesis on Quality, Electronic Properties and Environmental Stability of Individual Monolayer Ti_3C_2 MXene Flakes. *Advanced Electronic Materials* **2016**, *2* (12), 1600255.
(36) Cocker, T. L.; Titova, L. V.; Fourmaux, S.; Bandulet, H. C.; Brassard, D.; Kieffer, J. C.; El Khakani, M. A.; Hegmann, F. A. Terahertz conductivity of the metal-insulator transition in a nanogranular VO_2 film. *Appl. Phys. Lett.* **2010**, *97* (22), 221905.
(37) Baxter, J. B.; Schmuttenmaer, C. A. Carrier dynamics in bulk ZnO. I. Intrinsic conductivity measured by terahertz time-domain spectroscopy. *Phys. Rev. B: Condens. Matter Mater. Phys.* **2009**, *80* (23), DOI: 10.1103/PhysRevB.80.235205.
(38) Jepsen, P. U.; Cooke, D. G.; Koch, M. Terahertz spectroscopy and imaging−Modern techniques and applications. *Laser & Photonics Reviews* **2011**, *5* (1), 124−166.
(39) Ulbricht, R.; Hendry, E.; Shan, J.; Heinz, T. F.; Bonn, M. Carrier dynamics in semiconductors studied with time-resolved terahertz spectroscopy. *Rev. Mod. Phys.* **2011**, *83* (2), 543−586.
(40) Butler, K. T.; Dringoli, B. J.; Zhou, L.; Rao, P. M.; Walsh, A.; Titova, L. V. Ultrafast carrier dynamics in $BiVO_4$ thin film photoanode material: interplay between free carriers, trapped carriers and low-frequency lattice vibrations. *J. Mater. Chem. A* **2016**, *4* (47), 18516−18523.
(41) Titova, L. V.; Cocker, T. L.; Xu, S.; Baribeau, J.-M.; Wu, X.; Lockwood, D. J.; Hegmann, F. A. Ultrafast carrier dynamics and the role of grain boundaries in polycrystalline silicon thin films grown by molecular beam epitaxy. *Semicond. Sci. Technol.* **2016**, *31* (10), 105017.
(42) Lloyd-Hughes, J.; Jeon, T.-I. A Review of the Terahertz Conductivity of Bulk and Nano-Materials. *J. Infrared, Millimeter, Terahertz Waves* **2012**, *33* (9), 871−925.
(43) Cocker, T. L.; Baillie, D.; Buruma, M.; Titova, L. V.; Sydora, R. D.; Marsiglio, F.; Hegmann, F. A. Microscopic origin of the Drude-Smith model. *Phys. Rev. B: Condens. Matter Mater. Phys.* **2017**, *96* (20), 205439.
(44) Jensen, S. A.; Ulbricht, R.; Narita, A.; Feng, X.; Mullen, K.; Hertel, T.; Turchinovich, D.; Bonn, M. Ultrafast photoconductivity of graphene nanoribbons and carbon nanotubes. *Nano Lett.* **2013**, *13* (12), 5925−30.
(45) Guglietta, G. W.; Diroll, B. T.; Gaulding, E. A.; Fordham, J. L.; Li, S.; Murray, C. B.; Baxter, J. B. Lifetime, Mobility, and Diffusion of Photoexcited Carriers in Ligand-Exchanged Lead Selenide Nanocrystal Films Measured by Time-Resolved Terahertz Spectroscopy. *ACS Nano* **2015**, *9* (2), 1820−1828.
(46) Richter, C.; Schmuttenmaer, C. A. Exciton-like trap states limit electron mobility in TiO_2 nanotubes. *Nat. Nanotechnol.* **2010**, *5*, 769. https://www.nature.com/articles/nnano.2010.196#supplementary-information
(47) Alberding, B. G.; DeSario, P. A.; So, C. R.; Dunkelberger, A. D.; Rolison, D. R.; Owrutsky, J. C.; Heilweil, E. J. Static and Time-Resolved Terahertz Measurements of Photoconductivity in Solution-Deposited Ruthenium Dioxide Nanofilms. *J. Phys. Chem. C* **2017**, *121* (7), 4037−4044.
(48) Alberding, B. G.; Kushto, G. P.; Lane, P. A.; Heilweil, E. J. Reduced photoconductivity observed by time-resolved terahertz spectroscopy in metal nanofilms with and without adhesion layers. *Appl. Phys. Lett.* **2016**, *108* (22), 223104.
(49) Walther, M.; Cooke, D. G.; Sherstan, C.; Hajar, M.; Freeman, M. R.; Hegmann, F. A. Terahertz conductivity of thin gold films at the metal-insulator percolation transition. *Phys. Rev. B: Condens. Matter Mater. Phys.* **2007**, *76* (12), DOI: 10.1103/PhysRevB.76.125408.
(50) Titova, L. V.; Cocker, T. L.; Cooke, D. G.; Wang, X.; Meldrum, A.; Hegmann, F. A. Ultrafast percolative transport dynamics in silicon nanocrystal films. *Phys. Rev. B: Condens. Matter Mater. Phys.* **2011**, *83* (8), DOI: 10.1103/PhysRevB.83.085403.
(51) Hu, T.; Zhang, H.; Wang, J.; Li, Z.; Hu, M.; Tan, J.; Hou, P.; Li, F.; Wang, X. Anisotropic electronic conduction in stacked two-dimensional titanium carbide. *Sci. Rep.* **2015**, *5*, 16329. https://www.nature.com/articles/srep16329#supplementary-information
(52) Miranda, A.; Halim, J.; Barsoum, M. W.; Lorke, A. Electronic properties of freestanding $Ti_3C_2T_x$ MXene monolayers. *Appl. Phys. Lett.* **2016**, *108* (3), No. 033102.
(53) Seo, M. A.; Yim, J. H.; Ahn, Y. H.; Rotermund, F.; Kim, D. S.; Lee, S.; Lim, H. Terahertz electromagnetic interference shielding using single-walled carbon nanotube flexible films. *Appl. Phys. Lett.* **2008**, *93* (23), 231905.
(54) Liu, L.; Das, A.; Megaridis, C. M. Terahertz shielding of carbon nanomaterials and their composites − A review and applications. *Carbon* **2014**, *69*, 1−16.
(55) Dressel, M.; Grüner, G. *Electrodynamics of Solids: Optical Properties of Electrons in Matter*; Cambridge University Press: Cambridge, 2002.

DOI: 10.1021/acs.nanolett.9b04404
Nano Lett. 2020, 20, 636−643

(56) Mics, Z.; D'Angio, A.; Jensen, S. A.; Bonn, M.; Turchinovich, D. Density-dependent electron scattering in photoexcited GaAs in strongly diffusive regime. *Appl. Phys. Lett.* **2013**, *102* (23), 231120.
(57) Demsar, J.; Dekorsy, T. Carrier dynamics in bulk semiconductors and metals after ultrashort pulse excitation. In *Optical Techniques for Solid-State Materials Characterization*; 2016; pp 291–328.
(58) Block, A.; Liebel, M.; Yu, R.; Spector, M.; Sivan, Y.; García de Abajo, F. J.; van Hulst, N. F. Tracking ultrafast hot-electron diffusion in space and time by ultrafast thermomodulation microscopy. *Science Advances* **2019**, *5* (5), No. eaav8965.
(59) Smith, A. N.; Norris, P. M. Influence of intraband transitions on the electron thermoreflectance response of metals. *Appl. Phys. Lett.* **2001**, *78* (9), 1240–1242.
(60) Averitt, R. D.; Lobad, A. I.; Kwon, C.; Trugman, S. A.; Thorsmølle, V. K.; Taylor, A. J. Ultrafast Conductivity Dynamics in Colossal Magnetoresistance Manganites. *Phys. Rev. Lett.* **2001**, *87* (1), No. 017401.
(61) Hohlfeld, J.; Wellershoff, S. S.; Güdde, J.; Conrad, U.; Jähnke, V.; Matthias, E. Electron and lattice dynamics following optical excitation of metals. *Chem. Phys.* **2000**, *251* (1), 237–258.
(62) Ivanov, I.; Bonn, M.; Mics, Z.; Turchinovich, D. Perspective on terahertz spectroscopy of graphene. *EPL (Europhysics Letters)* **2015**, *111* (6), 67001.
(63) Jnawali, G.; Rao, Y.; Yan, H.; Heinz, T. F. Observation of a transient decrease in terahertz conductivity of single-layer graphene induced by ultrafast optical excitation. *Nano Lett.* **2013**, *13* (2), 524–30.
(64) Jensen, S. A.; Mics, Z.; Ivanov, I.; Varol, H. S.; Turchinovich, D.; Koppens, F. H. L.; Bonn, M.; Tielrooij, K. J. Competing Ultrafast Energy Relaxation Pathways in Photoexcited Graphene. *Nano Lett.* **2014**, *14* (10), 5839–5845.
(65) Hintermayr, V. A.; Polavarapu, L.; Urban, A. S.; Feldmann, J. Accelerated Carrier Relaxation through Reduced Coulomb Screening in Two-Dimensional Halide Perovskite Nanoplatelets. *ACS Nano* **2018**, *12* (10), 10151–10158.
(66) Gholivand, H.; Fuladi, S.; Hemmat, Z.; Salehi-Khojin, A.; Khalili-Araghi, F. Effect of surface termination on the lattice thermal conductivity of monolayer Ti3C2Tz MXenes. *J. Appl. Phys.* **2019**, *126* (6), No. 065101.
(67) Chen, L.; Shi, X.; Yu, N.; Zhang, X.; Du, X.; Lin, J. Measurement and Analysis of Thermal Conductivity of Ti3C2Tx MXene Films. *Materials* **2018**, *11* (9), 1701.
(68) Liu, R.; Li, W. High-Thermal-Stability and High-Thermal-Conductivity Ti3C2Tx MXene/Poly(vinyl alcohol) (PVA) Composites. *ACS Omega* **2018**, *3* (3), 2609–2617.
(69) Hemmat, Z.; Yasaei, P.; Schultz, J. F.; Hong, L.; Majidi, L.; Behranginia, A.; Verger, L.; Jiang, N.; Barsoum, M. W.; Klie, R. F.; Salehi-Khojin, A. Tuning Thermal Transport Through Atomically Thin Ti3C2Tz MXene by Current Annealing in Vacuum. *Adv. Funct. Mater.* **2019**, *29* (19), 1805693.
(70) Persson, I.; Näslund, L.-Å.; Halim, J.; Barsoum, M. W.; Darakchieva, V.; Palisaitis, J.; Rosen, J.; Persson, P. O. Å. On the organization and thermal behavior of functional groups on Ti3C2MXene surfaces in vacuum. *2D Mater.* **2018**, *5* (1), No. 015002.
(71) Karlsson, L. H.; Birch, J.; Halim, J.; Barsoum, M. W.; Persson, P. O. Å. Atomically Resolved Structural and Chemical Investigation of Single MXene Sheets. *Nano Lett.* **2015**, *15* (8), 4955–4960.
(72) Huang, S.; Mochalin, V. N. Hydrolysis of 2D Transition-Metal Carbides (MXenes) in Colloidal Solutions. *Inorg. Chem.* **2019**, *58* (3), 1958–1966.
(73) Naguib, M.; Unocic, R. R.; Armstrong, B. L.; Nanda, J. Large-scale delamination of multi-layers transition metal carbides and carbonitrides "MXenes. *Dalton Transactions* **2015**, *44* (20), 9353–9358.
(74) Voigt, C. A.; Ghidiu, M.; Natu, V.; Barsoum, M. W. Anion Adsorption, Ti3C2Tz MXene Multilayers, and Their Effect on Claylike Swelling. *J. Phys. Chem. C* **2018**, *122* (40), 23172–23179.
(75) Xiao, Z.; Yang, Q.; Huang, J.; Huang, Z.; Zhou, W.; Gao, Y.; Shu, R.; He, Z. Terahertz communication windows and their point-to-point transmission verification. *Appl. Opt.* **2018**, *57* (29), 8593–8593.

DOI: 10.1021/acs.nanolett.9b04404
Nano Lett. 2020, 20, 636–643